Cell and Tissue Research (2021) 385:21–35
https://doi.org/10.1007/s00441-021-03424-9

REGULAR ARTICLE

Development of epithelial cholinergic chemosensory cells of the urethra and trachea of mice

Alexander Perniss[1] · Patricia Schmidt[1] · Aichurek Soultanova[1] · Tamara Papadakis[1] · Katja Dahlke[2] · Anja Voigt[3] · Burkhard Schütz[4] · Wolfgang Kummer[1] · Klaus Deckmann[1]

Received: 17 June 2020 / Accepted: 24 January 2021 / Published online: 22 February 2021

Abstract

Cholinergic chemosensory cells (CCC) are infrequent epithelial cells with immunosensor function, positioned in mucosal epithelia preferentially near body entry sites in mammals including man. Given their adaptive capacity in response to infection and their role in combatting pathogens, we here addressed the time points of their initial emergence as well as their postnatal development from first exposure to environmental microbiota (i.e., birth) to adulthood in urethra and trachea, utilizing choline acetyltransferase (ChAT)-eGFP reporter mice, mice with genetic deletion of MyD88, toll-like receptor-2 (TLR2), TLR4, TLR2/TLR4, and germ-free mice. Appearance of CCC differs between the investigated organs. CCC of the trachea emerge during embryonic development at E18 and expand further after birth. Urethral CCC show gender diversity and appear first at P6-P10 in male and at P11-P20 in female mice. Urethrae and tracheae of MyD88- and TLR-deficient mice showed significantly fewer CCC in all four investigated deficient strains, with the effect being most prominent in the urethra. In germ-free mice, however, CCC numbers were not reduced, indicating that TLR2/4-MyD88 signaling, but not vita-PAMPs, governs CCC development. Collectively, our data show a marked postnatal expansion of CCC populations with distinct organ-specific features, including the relative impact of TLR2/4-MyD88 signaling. Strong dependency on this pathway (urethra) correlates with absence of CCC at birth and gender-specific initial development and expansion dynamics, whereas moderate dependency (trachea) coincides with presence of first CCC at E18 and sex-independent further development.

Keywords Brush cells · Tuft cells · Innate immunity · Toll-like receptors · MyD88 · Solitary chemosensory cells · Chemosensation

Introduction

Referring to their apical brush or tuft of stiff microvilli, identified in ultrastructural studies, a group of rare solitary epithelial cells has been initially termed brush or tuft cells (Rhodin and Dalhamn 1956; Sbarbati and Osculati 2005). Meanwhile, structural, histochemical, and single cell sequencing data revealed several unique characteristics defining distinct cell populations within and among organs (Deckmann et al. 2014; Krasteva et al. 2011; Montoro et al. 2018; Nadjsombati et al. 2018; Yamamoto et al. 2018). One of them is characterized by the expression of the acetylcholine synthesizing enzyme, choline acetyltransferase (ChAT), and the expression of the taste transduction signaling cascade, including the taste-specific G protein α-gustducin (GNAT3), phospholipase Cβ2 (PLCβ2), and the transient potential receptor cation channel subfamily M (melanostatin) member 5 (TRPM5). Such cholinergic

Alexander Perniss and Patricia Schmidt contributed equally to this work.

✉ Klaus Deckmann

[1] Institute for Anatomy and Cell Biology, German Center for Lung Research (DZL), Excellence Cluster Cardiopulmonary Institute (CPI), Justus-Liebig-University Giessen, Giessen, Germany

[2] Department of Gastroenterology, Infectious Diseases and Rheumatology, Charité Universitätsmedizin Berlin, Campus Benjamin Franklin, Berlin, Germany

[3] Max Rubner Laboratory, German Institute of Human Nutrition (DIfE), Nuthetal, Germany

[4] Institute of Anatomy and Cell Biology, Philipps-University, Marburg, Germany

chemosensory cells (CCC) have been identified in the upper airways (Saunders et al. 2014; Tizzano et al. 2011), the vomeronasal organ (Ogura et al. 2010), the auditory tube (Krasteva et al. 2012b), the trachea (Krasteva et al. 2011), the conjunctiva (Wiederhold et al. 2015), the gastro-intestinal tract including the gall bladder (Schutz et al. 2015), the urethra (Deckmann et al. 2014), and the thymus (Panneck et al. 2014). All cells of this category are closely related, even though there are organ-specific characteristics (Deckmann and Kummer 2016; Finger and Kinnamon 2011; Nadjsombati et al. 2018; O'Leary et al. 2019).

Their function is only partially identified. They utilize elements of the canonical taste transduction cascade to respond to potentially harmful substances including bacterial products (Deckmann et al. 2014; Finger et al. 2003; Krasteva et al. 2012a; Ogura et al. 2011; Saunders et al. 2014; Sbarbati et al. 2009; Tizzano et al. 2010) and helminths (Gerbe et al. 2016; Howitt et al. 2016; Nadjsombati et al. 2018; von Moltke et al. 2016). Upon activation, CCC initiate protective mechanisms like reflex inhibition of inspiratory activity (Krasteva et al. 2011; Tizzano et al. 2010) or stimulation of micturition (Deckmann et al. 2014), initiation of neurogenic inflammation (Saunders et al. 2014), and triggering type 2 immune responses (Bankova et al. 2018; Gerbe et al. 2016; Howitt et al. 2016; Nadjsombati et al. 2018; von Moltke et al. 2016). Accordingly, they have been attributed with a sentinel function and are regarded as crucial elements of the mucosal innate immune system (Krasteva and Kummer 2012; Kummer and Deckmann 2017; Middelhoff et al. 2017; Schneider et al. 2019; Tizzano and Finger 2013).

The transcription factor Skn-1a/Pou2f3 is required for CCC development, and its genetic deletion results in their absence in several organs (Ohmoto et al. 2013; Yamashita et al. 2017). Unlike taste cells in the taste buds, neither development nor maintenance of nasal CCC is dependent on intact innervation (Gulbransen et al. 2008). In postnatal life, CCC do undergo turnover like the surrounding epithelium, as initially demonstrated for the nose (Gulbransen and Finger 2005), and respond dynamically to challenges. While tracheal CCC have been described as "a stable population in a dynamic epithelium" under unchallenged conditions (Saunders et al. 2013), they increase markedly in numbers after exposure to house dust mites or mold in a leukotriene-dependent manner (Bankova et al. 2018). Severe infection with H1N1 influenza virus even provokes de novo appearance of solitary chemosensory cells (cholinergic traits not investigated in this study) in the murine distal lung, whereas such cells are not present in uninfected lungs (Rane et al. 2019). In the intestine, their number increases vastly in response to helminth and protozoan infection (Gerbe et al. 2016; Howitt et al. 2016; Nadjsombati et al. 2018; Schneider et al. 2018; von Moltke et al. 2016). At least in the intestine, CCC not only increase in numbers during infection but are also necessary for helminth clearance. Mice lacking TRPM5 remain infected with *Nippostrongylus brasiliensis*, whereas wildtype mice expel this helminth within 2 weeks (Nadjsombati et al. 2018). Given their adaptive capacity in response to infection and their role in combatting pathogens, we addressed the time points of their initial emergence as well as their postnatal development from first exposure to environmental microbiota (i.e., birth) to adulthood, utilizing ChAT-eGFP reporter mice and focusing upon tracheal, urethral, and, to a lesser extent, thymic CCC. The necessity of direct contact to living microbiota for the development of CCC was assessed by using germ-free mice. Since these mice are still exposed, e.g., via the food, to bacterial products and bacterial remains capable of triggering innate immune responses by activating toll-like receptors (TLRs), we also included MyD88 (myeloid differentiation primary response 88) knockout (KO) mice in this study. MyD88 is involved in downstream signaling of all TLRs, except TLR3, as well as the interleukin-1-receptor (Wang et al. 2014). As genetic loss of MyD88 indeed resulted in lower CCC numbers, we further included TLR2 and TLR4 single- and double-deficient mice to narrow down the spectrum of signaling pathways potentially being involved. TLR2 and TLR4 were chosen because of their well-known importance in the recognition of bacterial lipopeptides and lipoteichoic acids of Gram-positive bacteria in the case of TLR2 (Irvine et al. 2013) and lipopolysaccharides of Gram-negative bacteria in the case of TLR4 (Park et al. 2009).

Material and methods

Animals

ChAT-eGFP (B6.Cg-Tg(RP23-268L19-EGFP)2Mik/J; Stock No. 007902) mice were obtained from Jackson Laboratory (Bar Habor, ME, USA). A second ChAT-eGFP mouse strain (von Engelhardt et al. 2007) was exclusively used to assess CCC appearance during embryonic development. Mice were housed in the animal facilities of the Justus-Liebig-University Giessen or the Philipps-University Marburg under specific-pathogen-free (SPF) conditions (10 h dark, 14 h light), with free access to food and water.

Germ-free mice (C57BL/6N; germ-free; > 12 weeks) were obtained from the gnotobiotic animal facility of the German Institute of Human Nutrition, Potsdam-Rehbruecke, Germany. Gnotobiotic mice were maintained in positive-pressure isolators. Mice were housed individually in polycarbonate cages on irradiated wood chips (25 kGy) at 22 ± 2 °C and a relative humidity of 55 ± 5% on a 12 h light-dark cycle. All mice had unrestricted access to irradiated (50 kGy) experimental diets and autoclaved water throughout the experiment. Control mice (C57BL/6N, same

sex and age as germ-free mice; SPF) were obtained from Jackson Laboratory and housed at the animal facility of the Justus-Liebig-University Giessen in individually ventilated cages under SPF conditions. TLR2-KO (C57BL/10ScSn-TLR2^{tm1}), TLR4-def (C57BL/10ScN-TLR4 (spontaneous deletion of the *Trl4* gene)), and TLR2-KO/TLR4-def (C57BL10ScN-TLR4/TLR2^{tm1}) and corresponding wildtypes (TLR-WT; C57BL/10ScSn) were also obtained from the animal facility of the German Institute of Human Nutrition, Potsdam-Rehbruecke, Germany; all investigated mice of this strains were > 12 weeks old. These mice were bred as described previously (Heimesaat et al. 2007).

Tissues from MyD88-KO mice (B6.129-Myd88^{tm1}Aki; > 12 weeks) and corresponding wildtypes (MyD88-WT; litter mates of MyD88-KO mice) were obtained from two independent sources. The strain originally generated by Adachi et al. (1998) was bred and provided by Rainer Glauben, Charite Berlin, and by Axel Pagenstecher, Philipps-University Marburg.

This study was carried out in accordance with the recommendations of European Communities Council Directive of 24th November 1986 (86/609/EEC). The protocol was approved by the local authorities, i.e., Regierungspräsidium Giessen, Germany (reference no. 572_M, 571_M, 557_AZ, Ex-15–2018), the Office for Agriculture, Ecology, and Regional Planning of the State of Brandenburg (Germany) according to §8.1 Animal Welfare Act (approval number: 23-2347-6-2009 and 23-2347-24-2010), and the Landesamt für Gesundheit und Soziales (LAGESO), Berlin (approval number T0294/10).

3R statement

In this study, more than 450 tissue specimens were collected, investigated, and analyzed. In order to adhere to the 3R principle (reduction, replacement, and refinement in animal experiments principle (Russell and Burch 1959)) the number of animals used for this study was kept to a minimum by taking multiple organs (urethra, trachea, thymus) from the same animal and by taking specimens from animals that have been sacrificed for other purposes.

Immunohistochemistry and whole-mount immunostaining

Organs used for immunohistochemistry and whole-mount immunostaining were either freshly dissected and fixed by immersion or taken from animals fixed by transcardiac perfusion with 4% paraformaldehyde (in 0.1 M phosphate buffer, pH 7.4; both purchased from Carl Roth, Karlsruhe, Germany) or Zamboni solution (2% paraformaldehyde/15% saturated picric acid; Merck, Darmstadt, Germany, in 0.1 M phosphate buffer, pH 7.4), preceded by a flush with vascular rinsing solution (Forssmann et al. 1977). Organs were washed in 0.1 M phosphate buffer and embedded in paraffin (Paraplast Plus®, Leica, Nussloch, Germany) or incubated overnight in 18% sucrose (Carl Roth, Karlsruhe, Germany) in 0.1 M phosphate buffer, embedded in Tissue-Tek® O.C.T.™ Compound (Sakura Finetek Germany GmbH, Staufen, Germany) and frozen in liquid nitrogen. For immunostainings, tissue sections or whole-mounts of investigated strains were processed simultaneously with corresponding controls, e.g., wildtypes. Primary antibody was applied to 4–18 tissue sections (frozen 10 µm or paraffin 5 µm) from every organ. At least three animals per experimental setup were analyzed. For whole-mount immunostainings of tracheae, the trachea was dissected from the larynx to the bifurcation and the trachealis muscle was cut longitudinally. For whole-mount immunostainings of urethrae, the whole urethra was taken and cut longitudinally. The tracheae and urethrae were opened and fixed flat on a silicon elastomer (Dow Corning, Midland, MI, USA) with insect needles (Fiebig-Lehrmittel, Berlin, Germany). Specimens were permeabilized with 0.3% Triton X 100 (Carl Roth, Karlsruhe, Germany) for 2 h; unspecific protein binding sites were saturated by incubation with 4% horse serum (PAA Laboratories Inc., Pasching, Austria) and 1% bovine serum albumin (Sigma Aldrich/Merck, Darmstadt, Germany) in 0.005 M phosphate buffer for 2 h. Samples were incubated in primary and secondary antibodies overnight each, rinsed, post-fixed for 10 min in 4% paraformaldehyde, and mounted in Mowiol (Sigma Aldrich/Merck, Darmstadt, Germany) containing 4′,6-diamidino-2-phenylindol (DAPI, 1 µg/ml, Sigma Aldrich/Merck, Darmstadt, Germany).

To investigate prenatal development of CCC, embryos of ChAT-eGFP mice (von Engelhardt et al. 2007) were harvested at specified embryonic stages (E12, $N = 4$; E14, $N = 5$; E16, $N = 8$; E18, $N = 6$) and shortly after birth (P0, $N = 3$), which were determined by fertilization. After extraction, embryos were sacrificed, fixed by immersion with Zamboni solution, cut into halves, and embedded in paraffin. Embryos were sectioned (5 µm), and every 10th section was stained with H.E. or Giemsa for orientation. Every second section harboring tracheal epithelium was immunostained and analyzed.

Primary antibodies were chicken-anti-GFP (green fluorescent protein, NB100-1614, 1:4000 dilution; Novus Biologicals, Centennial, USA), goat-anti-ChAT (AB144P, 1:250 dilution; Merck Millipore/Merck, Darmstadt, Germany), rabbit-anti-DCAMKL1 (Serine/threonine-protein kinase DCLK1 (Doublecortin-like kinase 1)), ab31704 (1:2000 dilution; Abcam, Cambridge, UK), and rabbit-anti-TPRM5 (1:4000–8000 (Kaske et al. 2007)).

Secondary antibodies were donkey-anti-chicken IgG conjugated to fluorescein isothiocyanate (FITC; 703-095-155; 1:800; Dianova, Hamburg, Germany), donkey-anti-rabbit

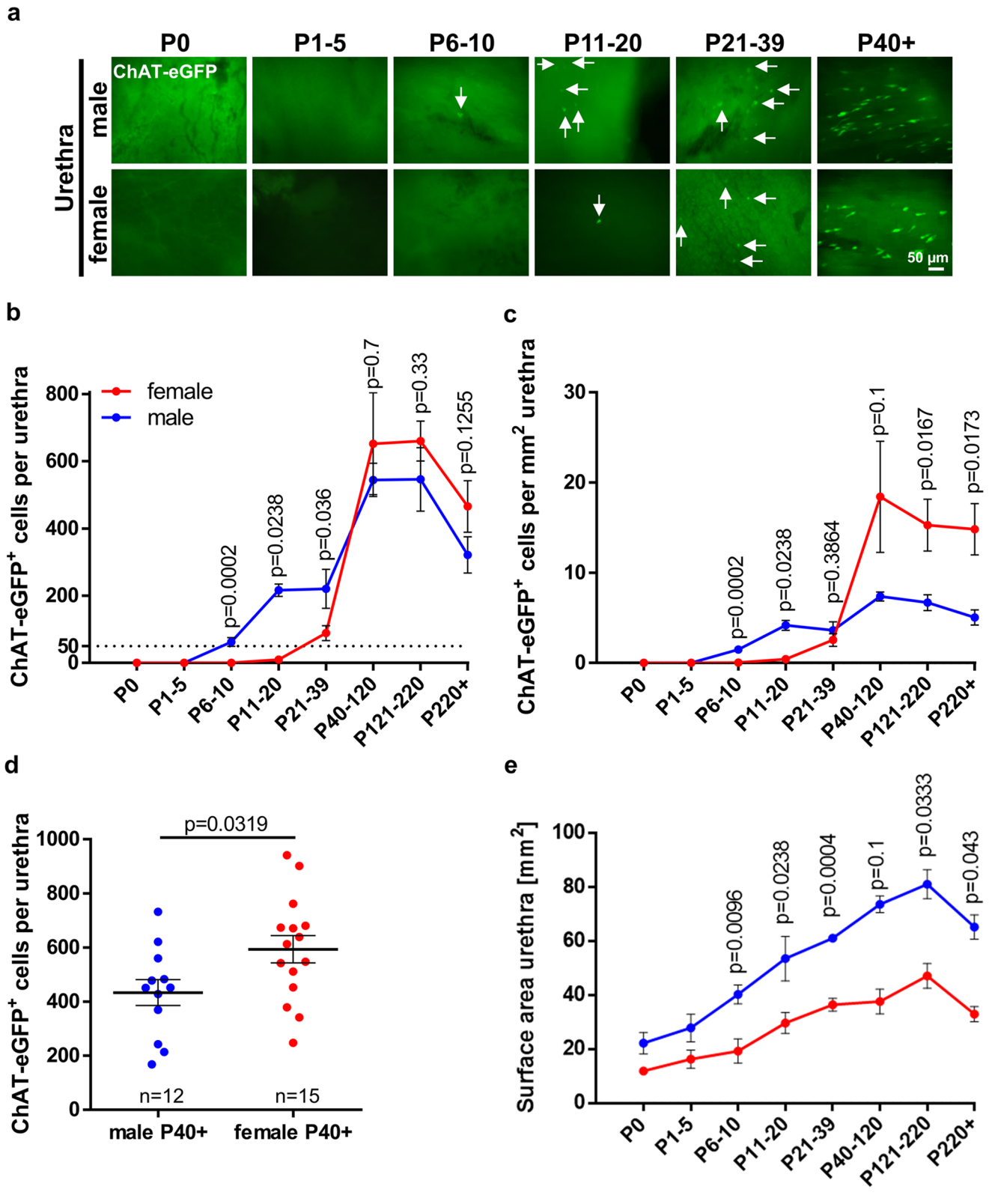

IgG conjugated to Cyanine 3 (Cy3; 2567112; 1:2000; Merck Millipore/Merck, Darmstadt, Germany), donkey-anti-rabbit IgG Alexa 488 (A21206; 1:500; Thermo Fisher Scientific Inc., Waltham, MA, USA), donkey-anti-goat IgG Alexa 488 (A11055; 1:1000; Thermo Fisher Scientific Inc., Waltham, MA, USA), and donkey-anti-goat IgG Cy3 (AP180C;

◂**Fig. 1** Postnatal development of CCC in the urethra. **a** Immunofluorescence using tissue from ChAT-eGFP mice, eGFP signal was antibody enhanced, representative images of female and male urethrae at different time points during postnatal development; arrows mark ChAT-eGFP-positive urethral CCC. **a** and **b** Quantitative analysis of ChAT-eGFP-positive cells per urethra **b** and per mm^2 **c** using whole-mount preparations in female and male mice at different time points during development; male: P0 $N = 5$; P1-5 $N = 8$; P6-10 $N = 17$; P11-20 $N = 3$; P21-39 $N = 6$; P40-120 $N = 3$; P121-220 $N = 3$; P250+ $N = 6$; female: P0 $N = 3$; P1-5 $N = 4$; P6-10 $N = 6$; P11-20 $N = 6$; P21-39 $N = 9$; P40-120 $N = 3$; P121-220 $N = 7$; P220+ $N = 5$. Dashed line marks cell count of 50 cells per urethra. **d** Numbers of ChAT-eGFP-positive cells per urethra in animals P40+, cumulative data of the three oldest age groups depicted in **b**; **e** Surface area of male and female urethrae used for generating **c**. **b**–**e** Graphs depict means and SEM. Blue: males, red: females. P-values were calculated with Mann-Whitney test

1:16,000; Merck Millipore/Merck, Darmstadt, Germany). Specificity of secondary reagents was validated by omission of primary antibodies.

CCC number in ChAT-eGFP mice was assessed by enhancement of endogenous eGFP signal with antibodies against eGFP. In C57BL/6N-mice, MyD88-KO mice, TLR-KO mice, TLR-def mice, and corresponding wildtypes, all not carrying the ChAT-eGFP reporter, CCC numbers were assessed by TRPM5-, ChAT-, or DCAMKL1-immunolabeling. To evaluate the degree of co-localization of ChAT-eGFP expression and TRPM5-immunoreactivity in CCC, the TRPM5-antibody was applied to whole-mounts (trachea and urethra) from ChAT-eGFP mice.

Sections and whole-mounts were evaluated by epifluorescence microscopy (Axioplan 2, Zeiss, Oberkochen, Germany) or with a confocal laser scanning microscope (LSM 710, Zeiss, Oberkochen, Germany). Overlay images were created using ImageJ (https://imagej.nih.gov/ij). For evaluation of cell numbers in tracheae and urethrae, we used whole-mount preparations and counted all positive cells in the organ manually or interactively using an ImageJ cell counter plug-in. Counting of a data set was performed by the same person to exclude experimenter dependent bias.

Surface area of trachea and urethra was calculated using ImageJ, except for adult tracheae of germ-free, control mice, MyD88-KO and MyD88-WT. In these cases, 8 pictures at × 10 magnification were taken along tracheal whole-mounts as illustrated in Supplementary Fig. 1a and used to evaluate CCC number per square millimeter. The number of CCC in TLR-deficient mice and corresponding wildtypes was evaluated using frozen or paraffin sections; here, the number of positive cells per millimeterbasal lamina was calculated utilizing the software Axiovision (Zeiss, Oberkochen, Germany) in case of the trachea (at least 10 longitudinal sections per animal were analyzed) or positive cells per section for the urethra (on average 25 sections per animal) were counted. To investigate appearance of CCC in thymi of different ages, at least 6 sections per animal ($N = 3$, mixed sexes) were analyzed.

Statistical analysis

Data were analyzed by Mann-Whitney test or Kruskal-Wallis test with GraphPad Prism 7 (GraphPad Software Inc., La Jolla, CA, USA). $P \leq 0.05$ were regarded as statistically significant.

Results

Sexual dimorphism of postnatal urethral CCC development

The time course of urethral CCC appearance showed a sexual dimorphism in ChAT-eGFP mice (Fig. 1). In male mice, urethral CCC appeared first between P6 and P10. In female mice, urethral CCC appeared first between P11 and P20. In both sexes, maximum urethral CCC numbers were reached between P40 and P220 and declined thereafter (Fig. 1b and c). Male mice had significantly higher absolute CCC numbers and CCC density per surface area than females in the periods P6–10, P11–20, and P21–39. In older animals (P40+), however, urethral CCC were more abundant in female mice (Fig. 1b, c, d; Supplementary Fig. 2). This gender difference was particularly pronounced in urethral CCC density, since the total urethral surface area was about 1.8 times larger in males than in females (Fig. 1e).

CCC of the trachea appear already during embryonic development

In ChAT-eGFP mice (von Engelhardt et al. 2007), CCC could not be detected within the tracheal epithelium at E12, E14, and E16. They appeared first at E18 in 5 of 6 investigated tracheae (Fig. 2), albeit in rare occurrence compared with pups sacrificed directly after birth (P0) (Figs. 2 and 3). Postnatal development was quantified in ChAT-eGFP (B6.Cg-Tg(RP23-268L19-EGFP)2Mik/J) mice. The number and density of tracheal CCC increased considerably until P78 (from 54 at P0 to 3950 cells at P78, Fig. 3a–c and Supplementary Fig. 1b and 3). In contrast to the urethra, no gender difference could be observed (Fig. 3b, c; Supplementary Fig. 1c). In tracheal whole-mount preparations of adult mice, about 89% of the cells labeled with TRPM5 antibody were also ChAT-eGFP-positive (Fig. 3d; Supplementary Fig. 3). In neonatal animals (P0-P2), however, only 45% of cells were double-positive ($p < 0.0004$, Mann-Whitney test). This co-localization increased further to 65% at P33 (Fig. 3e and f). The number of cells only positive for eGFP was extremely low in the tracheal epithelium throughout all ages.

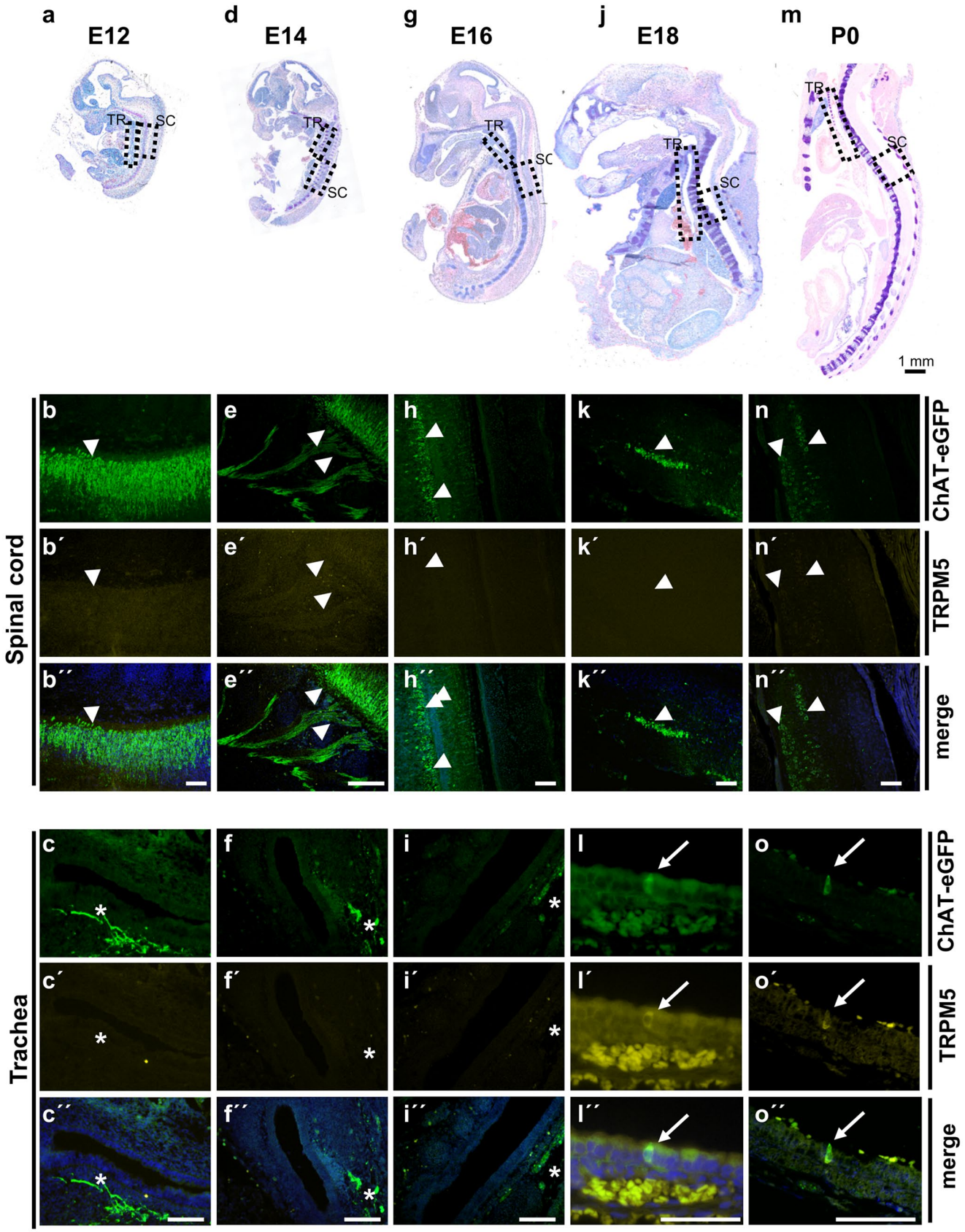
a
E12
d
E14
g
E16
j
E18
m
P0
TR
SC
1 mm
Spinal cord
Trachea
ChAT-eGFP
TRPM5
merge

◂**Fig. 2** Prenatal and perinatal development of tracheal CCC. Giemsa-stained paraffin sections from ChAT-eGFP mice (von Engelhardt et al. 2007) at distinct developmental stages with corresponding immunofluorescence images of trachea and spinal cord **a**–**c** E12 ($N = 4$), **d**–**f** E14 ($N = 5$), **g**–**i** E16 ($N = 8$), (j–l) E18 ($N = 6$), and (m–o) P0 ($N = 3$). Dashed boxes highlight locations where according immunofluorescence images of trachea (TR; **b**, **e**, **h**, **k**, and **n**) and spinal cord (SC; **c**, **f**, **i**, **l**, and **o**) were taken from adjacent sections double-labeled for TRPM5 and GFP; arrows mark ChAT-eGFP- and TRPM5-positive tracheal CCC at E18 and P0; arrowheads mark ChAT-eGFP-positive neurons; asterisks mark ChAT-eGFP-positive nerve fibers below the tracheal epithelium. Scale bar depicts 100 µm in the immunofluorescence images and 1 mm in Giemsa-stained overview images

TLR2/TLR4 and MyD88 deficiencies impair postnatal CCC expansion

We could not detect any urethral CCC in tissue sections from MyD88-KO mice stained with TRPM5 antibody (Supplementary Fig. 4a and b) and, hence, proceeded with whole-mount preparations using both TRPM5 and ChAT antibodies. TRPM5 antibody staining of urethral whole-mounts of adult ChAT-eGFP mice revealed about 99% congruency of ChAT-eGFP expression and TRPM5-immunolabeling antibody, justifying the use of TRPM5 antibody as a surrogate marker for urethral CCC (Supplementary Fig. 4c). Double staining of urethral whole-mount preparations from MyD88-KO mice and corresponding wildtypes with TRPM5 and ChAT antibodies also confirmed the near total coexistence of both signals (Fig. 4a and b). The total number of urethral CCC was significantly reduced by 69% in MyD88-KO mice compared with corresponding wildtypes (Fig. 4c). Since MyD88 is involved in downstream signaling of most TLRs (except TLR3), we reasoned that TLRs might be involved in the development of urethral CCC. We focused on TLR2 and TLR4 because of their importance in recognizing cell wall components of uropathogenic Gram-positive and -negative bacteria, respectively (Irvine et al. 2013; Park et al. 2009). Urethral sections from TLR2-KO, TLR4-def, and TLR2-KO/TLR4-def mice all showed significant reduction of TRMP5-immunoreactive cells by 88%, 88%, and 74%, respectively, when compared with corresponding wildtypes. However, no significant differences between the TLR-KO strains could be observed (Fig. 4d).

In tracheal whole-mount preparations, the congruency of staining with TRPM5 and ChAT antibodies was not 100%. $TRPM5^+/ChAT^-$ cells occurred in addition to double-labeled ($TRPM5^+/ChAT^+$) cells (Fig. 5a and b). Nevertheless, both stainings revealed significantly fewer CCC in MyD88-KO mice than in corresponding wildtypes (TRPM5: reduction by 36%, ChAT: reduction by 33%; Fig. 5c and d). Comparable results were also obtained with antibodies against DCAMKL1, another CCC marker, applied on TLR2-KO, TLR4-def, and TLR2-KO/TLR4-def tracheal sections (reduction of CCC by 47%, 29%, and 42%, respectively; Fig. 5e). DCAMKL1 was validated as a marker for CCC in tracheal whole-mount preparations of ChAT-eGFP mice, showing DCAMKL1-immunoreactivity in about 92% of all GFP-positive cells (Supplementary Fig. 5).

CCC develop independent of living microbiota

To determine whether the presence of living microbiota has impact on the development of CCC, germ-free C57BL/6 N mice were investigated. Selection of investigated time points was guided by the preceding experiments on urethrae of ChAT-eGFP mice, showing initial appearance and average cell count of about 50 cells per urethra on P7 in male and P33 in female mice, and highest numbers in both sexes in mice older than P100 (Fig. 1b). TRPM5-immunolabeling was utilized to investigate postnatal development of urethral CCC in germ-free versus SPF mice (Fig. 6a and b). Significantly more TRPM5-positive urethral CCC were counted on P7 in germ-free male mice, compared with SPF-housed C57BL/6 N mice (Fig. 6c; Supplementary Fig. 6a), but neither in P33 female mice (Fig. 6e; Supplementary Fig. 6c) nor in adult (P100+) mice of either sex (Fig. 6d, f; Supplementary Fig. 6b, d). In the trachea, we could not detect any difference in cell number between germ-free and SPF-housed control mice, neither in young (P7 [male] and P33 [female]), nor in adult mice (both genders) (Fig. 7).

Thymic CCC

In the course of our studies, we obtained some qualitative observations on thymic CCC. They were present already at birth (Supplementary Fig. 7), in adult MyD88-KO and TLR2/4-deficient mice (Supplementary Fig. 8), and in thymi of germ-free mice at the investigated time points, i.e., P7, P33, and P100+ (Supplementary Fig. 9).

Discussion

The present data reveal a perinatal appearance and postnatal expansion of CCC with distinct organ-specific onset in development, sexual dimorphism, and dependency on pattern recognition receptor signaling. This time course of development renders a significant role of this cell type in intrauterine organ development unlikely, and rather points towards an onset of function in postnatal life. Accordingly, mucosal CCC are generally considered as sentinels monitoring luminal content for potentially harmful substances, predominantly of microbial origin (Deckmann and Kummer 2016; Finger and Kinnamon 2011; Krasteva and Kummer 2012;

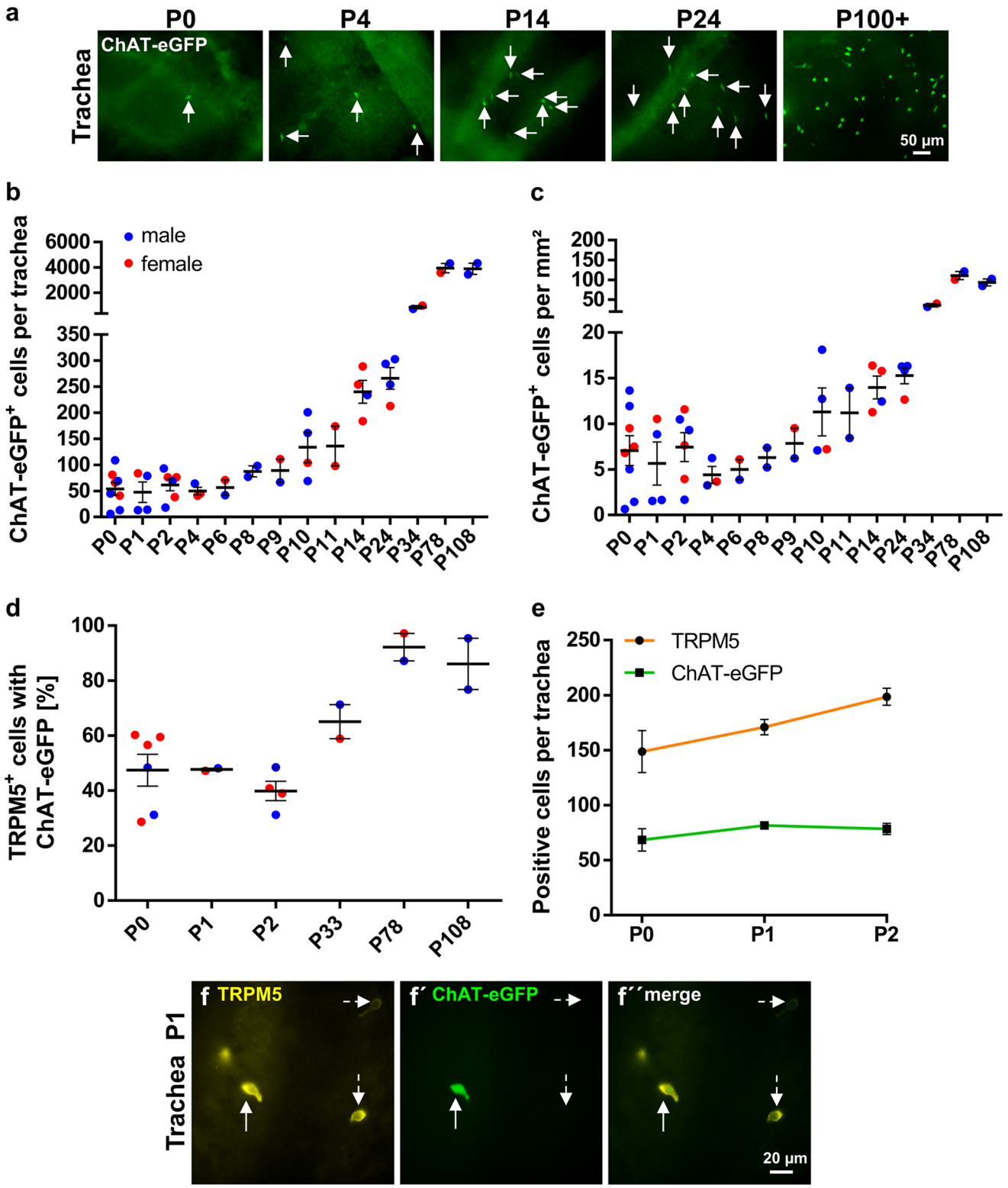

Kummer and Deckmann 2017; Schneider et al. 2019; Ting and von Moltke 2019; Tizzano and Finger 2013), to which exposure begins after birth. The present data also indicate at least a modulating and enhancing influence of the developing microbiota on the postnatal population dynamics of CCC, albeit microbiota are not an absolute requirement for the occurrence of CCC. This conclusion is based on our experiments with MyD88-KO

◂**Fig. 3** Postnatal development of CCC in the trachea. **a** Immunofluorescence with GFP antibody using tissue from ChAT-eGFP mice, representative images of tracheae at different time points during postnatal development; arrows point to ChAT-eGFP-positive tracheal CCC. GFP-positive cells were counted in tracheal whole-mount preparations; absolute numbers are given in **b**, cell number per mm^2 is shown in **c**. **d** Percentage of TRPM5-positive cells which also were positive for ChAT-eGFP from same animals as in **b** and **c**. **e** Total number of TRPM5- and ChAT-eGFP-positive cells at P0–P2 from same animals as in **b** and **c** ($N = 2$–6 each time point). **f** Representative immunofluorescence pictures with antibodies against TRPM5 and GFP of a tracheal whole-mount from an one day old ChAT-eGFP animal; dashed arrows mark a TRPM5 single-positive cell; solid arrows mark a TRPM5 and ChAT-eGFP double-positive cell. Graphs depict mean and SEM; **b**–**d** all data points depicted in scatter plots. Blue: males, red: females

and TLR-deficient mice. TLR2 and TLR4 are necessary for the detection of lipopeptides from bacterial origin and lipoteichoic acids or lipopolysaccharides from Gram-positive bacteria or Gram-negative bacteria, respectively, (Irvine et al. 2013; Park et al. 2009), and MyD88 is an essential downstream component of all TLR signaling except TLR3 (Wang et al. 2014). Genetic deletion of either of these components essentially reduced the number of CCC in the urethra and, to a lesser extent, in the trachea.

Likewise, MyD88 is also required for the induction of ChAT expression in lymphocytes (Reardon et al. 2013). Gnotobiotic mice are still exposed to TLR agonists, e.g., through their food and bedding material, and MyD88 expression was even found to be enhanced in the intestine of gnotobiotic mice compared with SPF mice (Yamamoto et al. 2012). This is consistent with our observation of generally unreduced and even enhanced numbers of CCC in male P7 urethra. These findings demonstrate that CCC development is independent of viability-associated

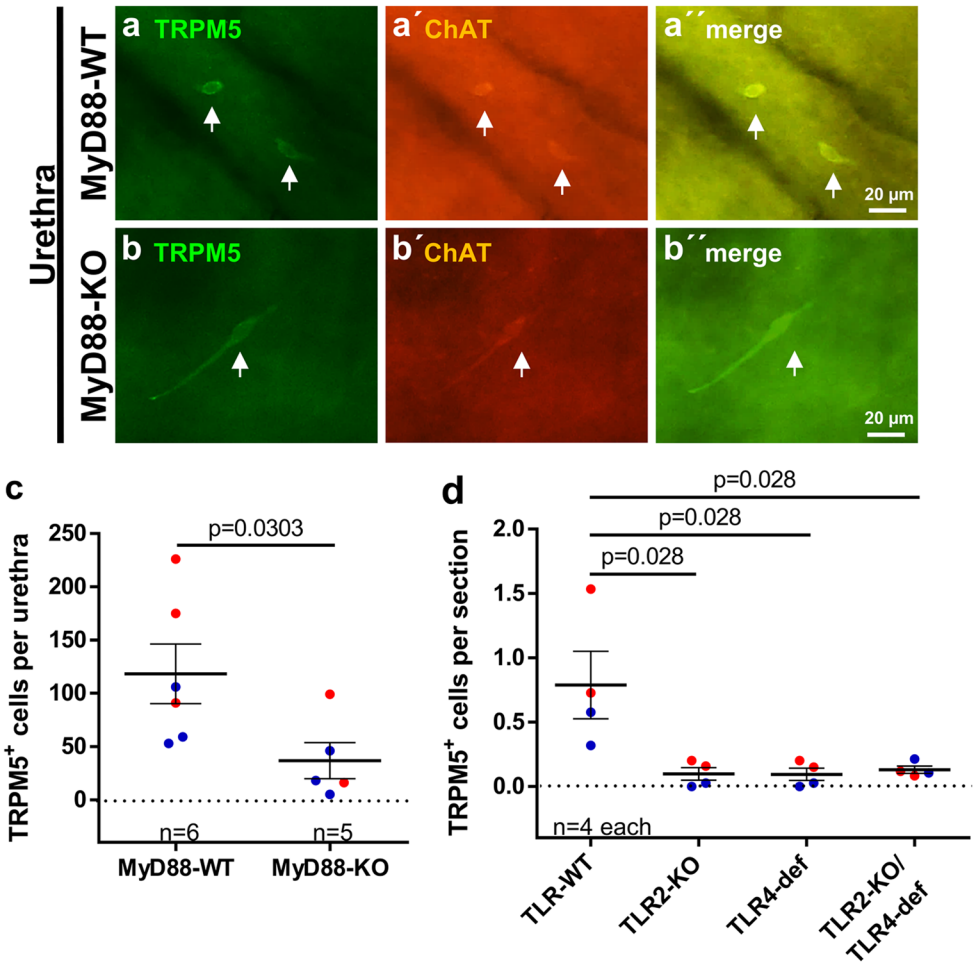

Fig. 4 Urethral CCC in MyD88-KO, TLR2-KO, TLR4-def, and TLR2-KO/TLR4-def mice. **a** and **b** Representative pictures of TRPM5 and ChAT double-labeled CCC (arrows) in urethral whole-mounts of MyD88-WT **a** and MyD88-KO **b** mice; all examples taken from P100+ mice. **c** Quantitative analysis of TRPM5-positive cells per urethra counted at whole-mount preparations as shown in **a** and **b**. **d** Number of TRPM5-positive cells in urethral tissue sections of TLR2-KO, TLR4-def, TLR2-KO/TLR4-def, and TLR-WT mice. Each data point represents the average number of cells from 20 sections from one animal. Bars and whiskers depict mean and SEM. Blue: males, red: females. All investigated animals were adult (> 12 weeks). *P* values were calculated with Mann-Whitney test

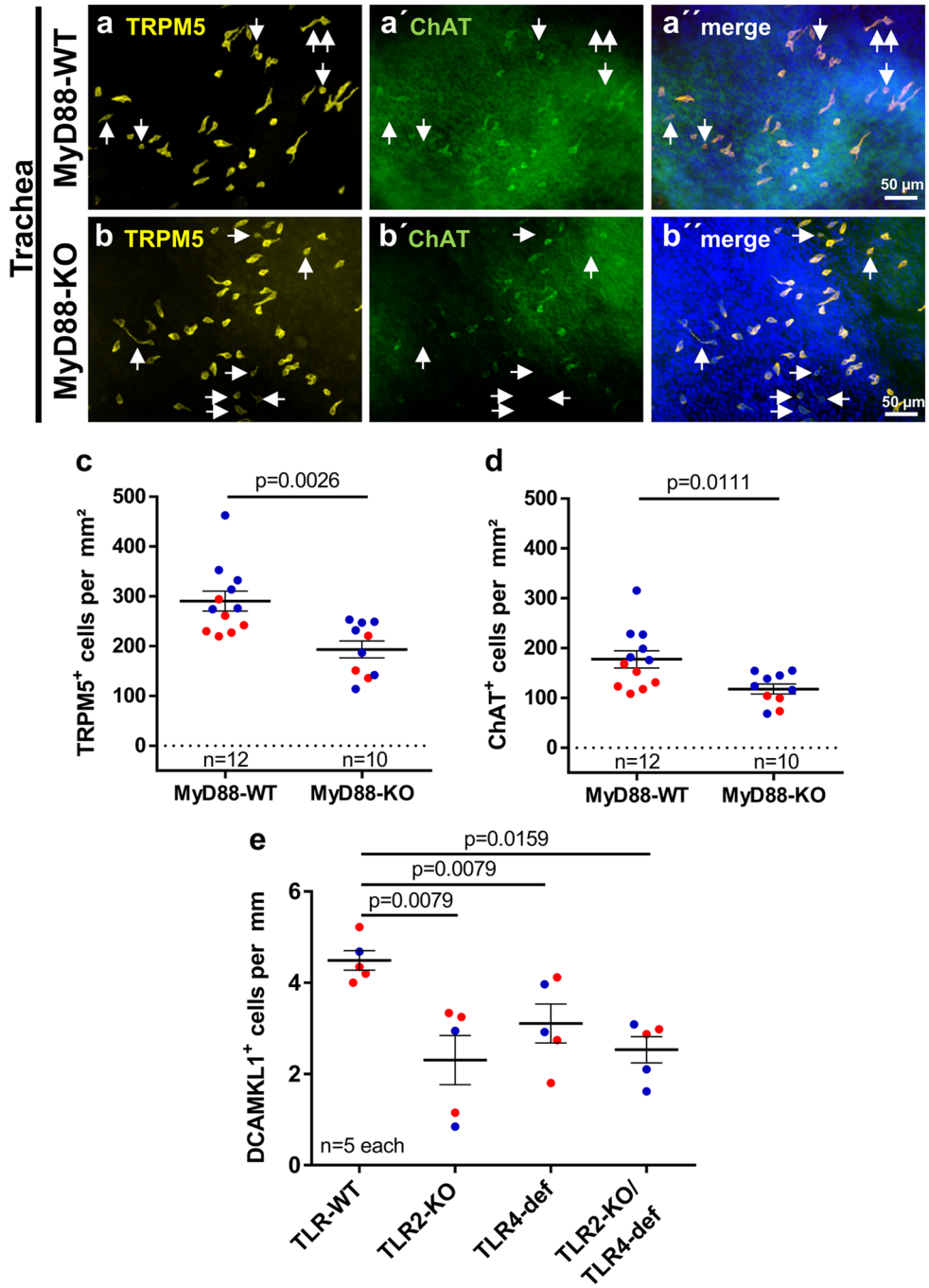

Fig. 5 Tracheal CCC in MyD88-KO, TLR2-KO, TLR4-def, and TLR2-KO/TLR4-def mice. **a** and **b** Double-labeling immunofluorescence of tracheal whole-mounts of MyD88-WT **a** and MyD88-KO **b** mice with antibodies against TRPM5 (yellow) and ChAT (green). Double-labeled cells dominate, single-labeled CCC ($TRPM5^+$/$ChAT^-$) are marked with arrows. **c** and **d** Densities of TRPM5-positive cells **c** and ChAT-positive cells **c** counted from whole-mounts as shown in **a** and **b**. **e** Number of DCAMKL1-positive cells per mm of basal lamina in tracheal tissue sections of TLR2-KO, TLR4-def, TLR2-KO/TLR4-def, and TLR-WT mice. Each data point represents a single animal analyzed with an average number of 20 single sections. Bars and whiskers depict mean and SEM. Blue: males, red: females. All investigated animals were adult (> 12 weeks). *P* values were calculated with Mann-Whitney test

pathogen-associated molecular patterns (vita PAMPs, (Sander et al. 2011)), but controlled by TLR2/4 signaling.

Although genetic deletion of TLR2, TLR4, TLR2/4, or MyD88 led to significantly reduced CCC numbers in the trachea, still more than 50% of CCC remained, pointing towards a CCC-inducing stimulus independent of pattern recognition signaling. This notion is supported by the presence of low basal numbers of CCC at birth (P0),

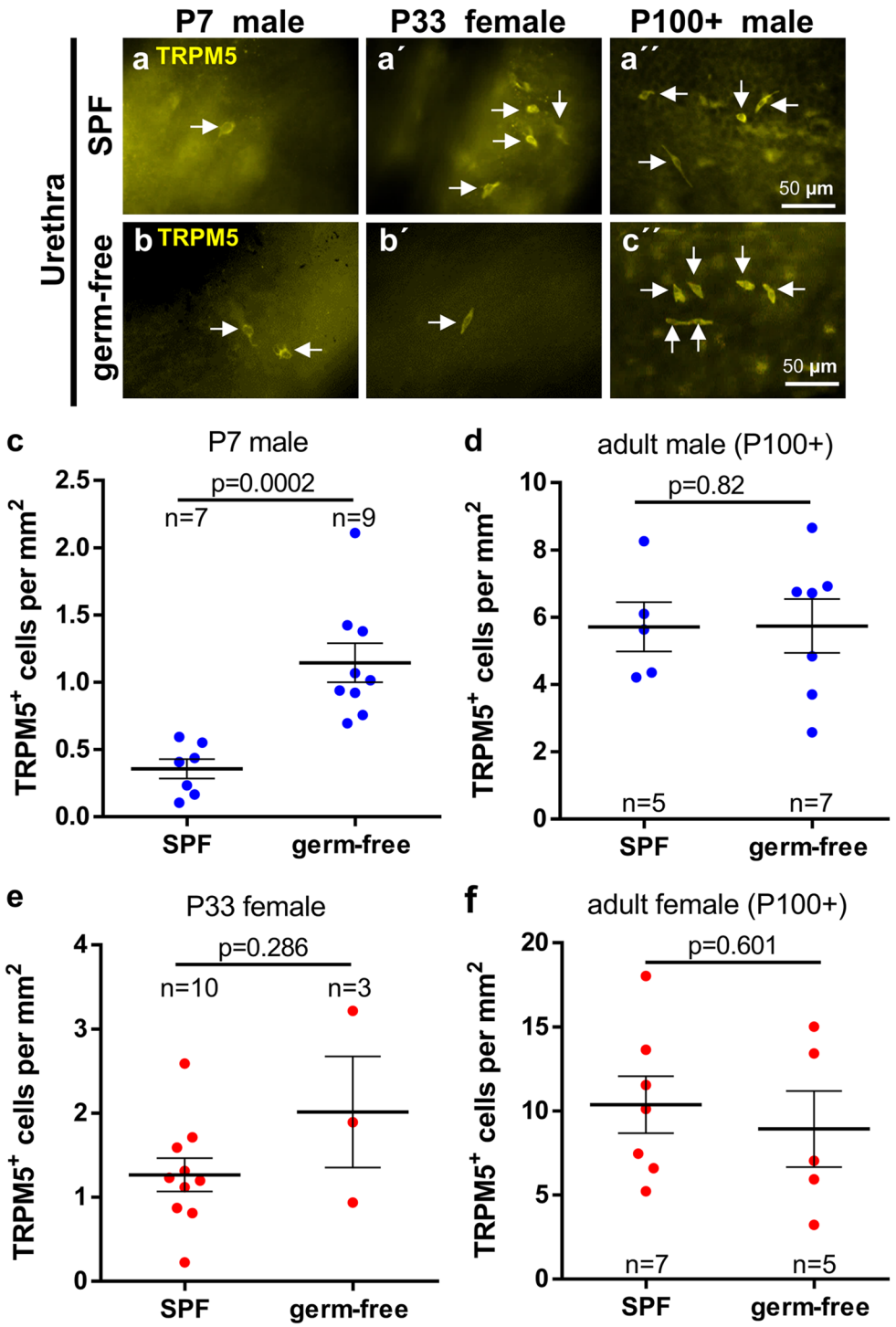

Fig. 6 Postnatal development of urethral CCC in germ-free versus SPF mice. **a** and **b** Representative immunofluorescence pictures, TRPM5-immunolabeling of urethral whole-mounts of SPF **a** and germ-free **b** mice**. c**–**f** Quantitative analysis of whole-mounts shown in **a** and **b**. Bars and whiskers depict mean and SEM. Blue: males, red: females. All investigated animals were adult (> 12 weeks). *P* values were calculated with Mann-Whitney test

prior to microbial contact. In line with our findings, early occurrence of chemosensory cells in the murine tracheal epithelium has also been described in TRPM5-GFP (P5, earlier time points not investigated; Saunders et al. 2013) and Tas2R131-GFP reporter mice (P3, earlier time points not investigated; Voigt et al. 2015). Similarly,

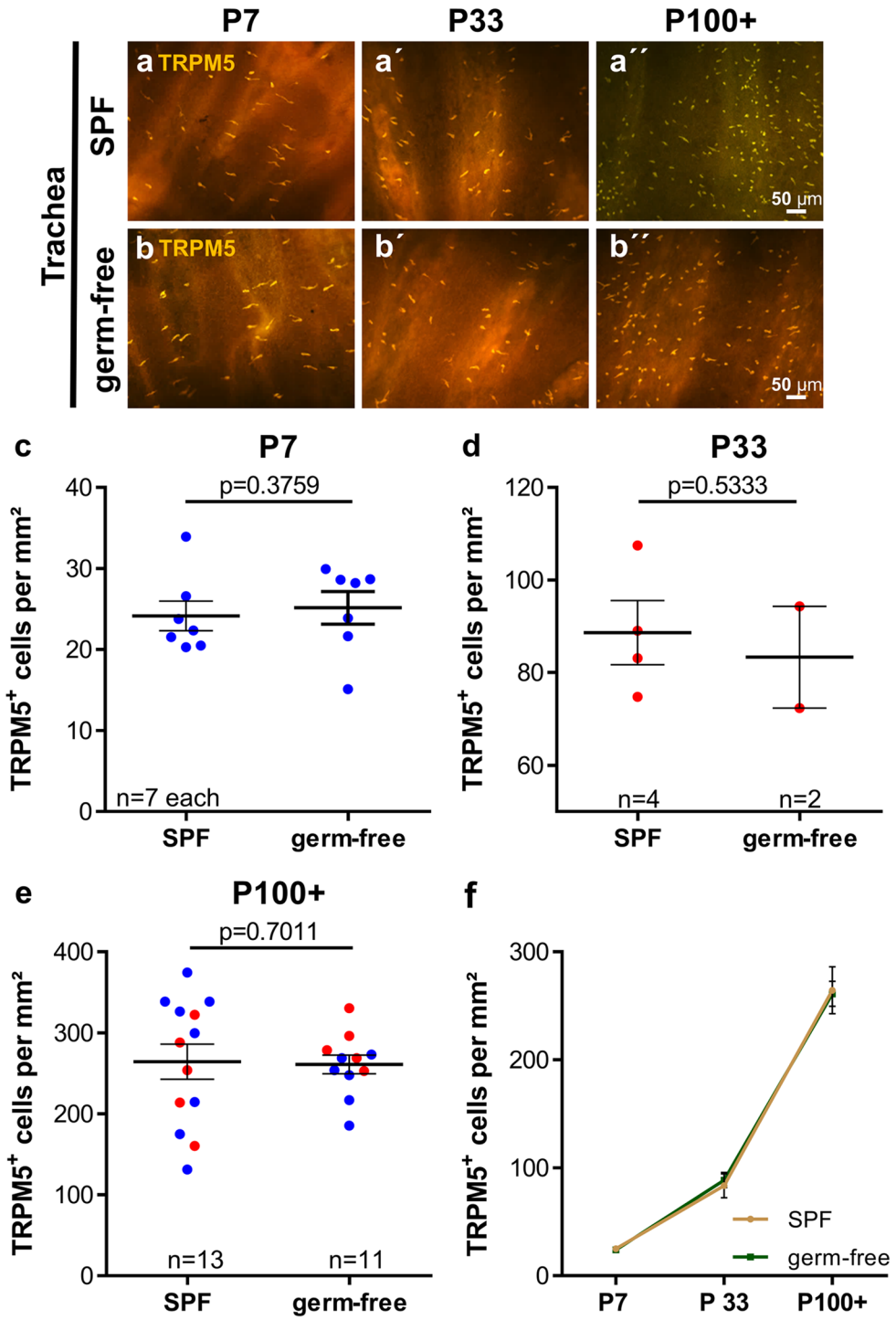

Fig. 7 Postnatal development of tracheal CCC in germ-free versus SPF mice. **a** and **b** Representative immunofluorescence pictures, TRPM5-immunolabeling of tracheal whole-mounts. **c**–**e** Quantitative analysis of whole-mounts shown in **a** and **b**, **f** visualization of data shown in **c**–**e** over time. Graphs depict means and SEM. Blue: males, red: females. All investigated animals were adult (> 12 weeks). *P* values were calculated with Mann-Whitney test

we observed considerable numbers of CCC, albeit not quantified, in the thymic medulla of MyD88-KO, TLR2-KO/TLR4-def, and germ-free mice. They were also present at birth, consistent with the observation of Tas2R131-GFP$^+$ and GNAT3-immunoreactive cells in the thymus at P3 (Voigt et al. 2015).

In contrast, genetic deletion of TLR2, TLR4, or MyD88 drastically reduced CCC numbers in the urethra by 69–88% compared with corresponding wildtypes and this coincided with lack of urethral CCC at birth. This strongly suggests that postnatal contact to TLR2/4 agonists, derived from the microbiome under physiological conditions, is required for CCC development in the urethra. MyD88 expression is regulated by estrogens (Zheng et al. 2006), and the downstream signaling proteins of the TLR4-MyD88 pathway, Bruton tyrosine kinase (BTK), and IL-1 receptor associated kinase (IRAK)1 are encoded by the X-chromosome (Spolarics 2007) with the consequence of higher IRAK1 levels in umbilical cord blood of female neonates compared with males (O'Driscoll et al. 2017). This has been considered one of the causes of sex-specific responses to infection and subsequent immunological advantage in female neonates (O'Driscoll et al. 2017). Notably, we also observed gender-specific differences in the first postnatal appearance of urethral CCC, which is also governed by TLR2/4-MyD88 signaling. It is tempting to assume a causal relationship, but this still needs to be experimentally addressed, in particular, since higher IRAK1 levels in females would predict earlier appearance of UCCC in females rather than in males. Consistent with this hypothesis, postnatal appearance and gender-specific developmental dynamics have also been reported for a closely related cell type, the brush cell of the rat common bile duct. It can be first detected by scanning electron microscopy at 4 weeks after birth and, thereafter, shows a remarkable increase in numbers, with a gender specific difference in time, i.e., between 8 and 12 weeks in the male and between 10 and 14 weeks in the female (Iseki 1991).

Collectively, our data show a marked postnatal expansion of CCC populations with distinct organ-specific features, including the relative impact of TLR2/4-MyD88 signaling. Strong dependency on this pathway (urethra) correlates with absence of CCC at birth and gender-specific initial development and expansion dynamics, whereas moderate dependency (trachea) coincides with presence of first CCC at E18 and sex-independent further development.

Supplementary information The online version contains supplementary material available at https://doi.org/10.1007/s00441-021-03424-9.Acknowledgements We thank Martin Bodenbenner, Theresa Eiffert, and Stefanie Demgensky for skillful technical assistance. We thank Rainer Glauben, Charite Berlin, and Axel Pagenstecher, Philipps-University Marburg, for providing the MyD88-knockout animals. We thank Vladimir Chubanov and Thomas Gudermann, Ludwig-Maximilian-University Munich, for providing TRPM5 antibody. We also thank Claudia Dames, Charite Berlin, for organizational assistance.

Author contribution AP and KD (Klaus Deckmann) designed research and performed statistical analysis. AP, KD, PS, AS, BS, and TP performed research and analyzed data. AV and DK (Katja Dahlke) designed animals. KD, AS, and WK obtained funding. KD, AP, PS, and WK drafted the manuscript. Work was supervised by WK and KD.

Funding Open Access funding enabled and organized by Projekt DEAL. This work was supported by a University Hospital of Giessen and Marburg (UKGM)-Justus-Liebig-University (JLU)-Cooperation Grant (# 7/2016 GI to KD), the German Research Foundation (SFB-TR84; project A6 to WK), SCHU1259/10-1 to BS, the German Center for Lung Research (DZL ALI-1.1 to WK) the Excellence Cluster Cardiopulmonary Institute (CPI, EXC 147 to WK), a Young Researcher Grant of the Faculty of Medicine, JLU Giessen (to AS), and the Else Kröner-Fresenius-Stiftung (2016_A90 to KD).

Declarations

Conflict of interest The authors declare that they have no conflict of interest.

References

Adachi O, Kawai T, Takeda K, Matsumoto M, Tsutsui H, Sakagami M, Nakanishi K, Akira S (1998) Targeted disruption of the MyD88 gene results in loss of IL-1- and IL-18-mediated function. Immunity 9:143–150

Bankova LG, Dwyer DF, Yoshimoto E, Ualiyeva S, McGinty JW, Raff H, von Moltke J, Kanaoka Y, Frank Austen K, Barrett NA (2018) The cysteinyl leukotriene 3 receptor regulates expansion of IL-25-producing airway brush cells leading to type 2 inflammation. Sci Immunol 3

Deckmann K, Filipski K, Krasteva-Christ G, Fronius M, Althaus M, Rafiq A, Papadakis T, Renno L, Jurastow I, Wessels L, Wolff M, Schutz B, Weihe E, Chubanov V, Gudermann T, Klein J, Bschleipfer T, Kummer W (2014) Bitter triggers acetylcholine release from polymodal urethral chemosensory cells and bladder reflexes. Proc Natl Acad Sci U S A 111:8287–8292

Deckmann K, Kummer W (2016) Chemosensory epithelial cells in the urethra: sentinels of the urinary tract. Histochem Cell Biol 146:673–683

Finger TE, Bottger B, Hansen A, Anderson KT, Alimohammadi H, Silver WL (2003) Solitary chemoreceptor cells in the nasal cavity serve as sentinels of respiration. Proc Natl Acad Sci U S A 100:8981–8986

Finger TE, Kinnamon SC (2011) Taste isn't just for taste buds anymore. F1000 Biol Rep 3:20

Forssmann WG, Ito S, Weihe E, Aoki A, Dym M, Fawcett DW (1977) An improved perfusion fixation method for the testis. Anat Rec 188:307–314

Gerbe F, Sidot E, Smyth DJ, Ohmoto M, Matsumoto I, Dardalhon V, Cesses P, Garnier L, Pouzolles M, Brulin B, Bruschi M, Harcus Y, Zimmermann VS, Taylor N, Maizels RM, Jay P (2016) Intestinal epithelial tuft cells initiate type 2 mucosal immunity to helminth parasites. Nature 529:226–230

Gulbransen BD, Clapp TR, Finger TE, Kinnamon SC (2008) Nasal solitary chemoreceptor cell responses to bitter and trigeminal stimulants in vitro. J Neurophysiol 99:2929–2937

Gulbransen BD, Finger TE (2005) Solitary chemoreceptor cell proliferation in adult nasal epithelium. J Neurocytol 34:117–122

Heimesaat MM, Fischer A, Siegmund B, Kupz A, Niebergall J, Fuchs D, Jahn HK, Freudenberg M, Loddenkemper C, Batra A, Lehr HA, Liesenfeld O, Blaut M, Gobel UB, Schumann RR, Bereswill S (2007) Shift towards pro-inflammatory intestinal bacteria aggravates acute murine colitis via Toll-like receptors 2 and 4. PLoS One 2:e662

Howitt MR, Lavoie S, Michaud M, Blum AM, Tran SV, Weinstock JV, Gallini CA, Redding K, Margolskee RF, Osborne LC, Artis D, Garrett WS (2016) Tuft cells, taste-chemosensory cells, orchestrate parasite type 2 immunity in the gut. Science 351:1329–1333

Irvine KL, Hopkins LJ, Gangloff M, Bryant CE (2013) The molecular basis for recognition of bacterial ligands at equine TLR2, TLR1 and TLR6. Vet Res 44:50

Iseki S (1991) Postnatal development of the brush cells in the common bile duct of the rat. Cell Tissue Res 266:507–510

Kaske S, Krasteva G, Konig P, Kummer W, Hofmann T, Gudermann T, Chubanov V (2007) TRPM5, a taste-signaling transient receptor potential ion-channel, is a ubiquitous signaling component in chemosensory cells. BMC Neurosci 8:49

Krasteva G, Canning BJ, Hartmann P, Veres TZ, Papadakis T, Muhlfeld C, Schliecker K, Tallini YN, Braun A, Hackstein H, Baal N, Weihe E, Schutz B, Kotlikoff M, Ibanez-Tallon I, Kummer W (2011) Cholinergic chemosensory cells in the trachea regulate breathing. Proc Natl Acad Sci U S A 108:9478–9483

Krasteva G, Canning BJ, Papadakis T, Kummer W (2012) Cholinergic brush cells in the trachea mediate respiratory responses to quorum sensing molecules. Life Sci 91:992–996

Krasteva G, Hartmann P, Papadakis T, Bodenbenner M, Wessels L, Weihe E, Schutz B, Langheinrich AC, Chubanov V, Gudermann T, Ibanez-Tallon I, Kummer W (2012) Cholinergic chemosensory cells in the auditory tube. Histochem Cell Biol 137:483–497

Krasteva G, Kummer W (2012) "Tasting" the airway lining fluid. Histochem Cell Biol 138:365–383

Kummer W, Deckmann K (2017) Brush cells, the newly identified gatekeepers of the urinary tract. Curr Opin Urol 27:85–92

Middelhoff M, Westphalen CB, Hayakawa Y, Yan KS, Gershon MD, Wang TC, Quante M (2017) Dclk1-expressing tuft cells: critical modulators of the intestinal niche? Am J Physiol Gastrointest Liver Physiol 313:G285–G299

Montoro DT, Haber AL, Biton M, Vinarsky V, Lin B, Birket SE, Yuan F, Chen S, Leung HM, Villoria J, Rogel N, Burgin G, Tsankov AM, Waghray A, Slyper M, Waldman J, Nguyen L, Dionne D, Rozenblatt-Rosen O, Tata PR, Mou H, Shivaraju M, Bihler H, Mense M, Tearney GJ, Rowe SM, Engelhardt JF, Regev A, Rajagopal J (2018) A revised airway epithelial hierarchy includes CFTR-expressing ionocytes. Nature 560:319–324

Nadjsombati MS, McGinty JW, Lyons-Cohen MR, Jaffe JB, DiPeso L, Schneider C, Miller CN, Pollack JL, Nagana Gowda GA, Fontana MF, Erle DJ, Anderson MS, Locksley RM, Raftery D, von Moltke J (2018) Detection of Succinate by Intestinal Tuft Cells Triggers a Type 2 Innate Immune Circuit. Immunity 49(33–41):e37

O'Driscoll DN, De Santi C, McKiernan PJ, McEneaney V, Molloy EJ, Greene CM (2017) Expression of X-linked Toll-like receptor 4 signaling genes in female vs. male neonates. Pediatr Res 81:831–837

O'Leary CE, Schneider C, Locksley RM (2019) Tuft cells-systemically dispersed sensory epithelia integrating immune and neural circuitry. Annu Rev Immunol 37:47–72

Ogura T, Krosnowski K, Zhang L, Bekkerman M, Lin W (2010) Chemoreception regulates chemical access to mouse vomeronasal organ: role of solitary chemosensory cells. PLoS One 5:e11924

Ogura T, Szebenyi SA, Krosnowski K, Sathyanesan A, Jackson J, Lin W (2011) Cholinergic microvillous cells in the mouse main olfactory epithelium and effect of acetylcholine on olfactory sensory neurons and supporting cells. J Neurophysiol 106:1274–1287

Ohmoto M, Yamaguchi T, Yamashita J, Bachmanov AA, Hirota J, Matsumoto I (2013) Pou2f3/Skn-1a is necessary for the generation or differentiation of solitary chemosensory cells in the anterior nasal cavity. Biosci Biotechnol Biochem 77:2154–2156

Panneck AR, Rafiq A, Schutz B, Soultanova A, Deckmann K, Chubanov V, Gudermann T, Weihe E, Krasteva-Christ G, Grau V, del Rey A, Kummer W (2014) Cholinergic epithelial cell with chemosensory traits in murine thymic medulla. Cell Tissue Res 358:737–748

Park BS, Song DH, Kim HM, Choi BS, Lee H, Lee JO (2009) The structural basis of lipopolysaccharide recognition by the TLR4-MD-2 complex. Nature 458:1191–1195

Rane CK, Jackson SR, Pastore CF, Zhao G, Weiner AI, Patel NN, Herbert DR, Cohen NA, Vaughan AE (2019) Development of solitary chemosensory cells in the distal lung after severe influenza injury. Am J Physiol Lung Cell Mol Physiol

Reardon C, Duncan GS, Brustle A, Brenner D, Tusche MW, Olofsson PS, Rosas-Ballina M, Tracey KJ, Mak TW (2013) Lymphocyte-derived ACh regulates local innate but not adaptive immunity. Proc Natl Acad Sci U S A 110:1410–1415

Rhodin J, Dalhamn T (1956) Electron microscopy of the tracheal ciliated mucosa in rat. Z Zellforsch Mikrosk Anat 44:345–412

Russell WMS, Burch RL (1959) The principles of humane experimental technique. Anim Welf Wheathampstead

Sander LE, Davis MJ, Boekschoten MV, Amsen D, Dascher CC, Ryffel B, Swanson JA, Muller M, Blander JM (2011) Detection of prokaryotic mRNA signifies microbial viability and promotes immunity. Nature 474:385–389

Saunders CJ, Christensen M, Finger TE, Tizzano M (2014) Cholinergic neurotransmission links solitary chemosensory cells to nasal inflammation. Proc Natl Acad Sci U S A 111:6075–6080

Saunders CJ, Reynolds SD, Finger TE (2013) Chemosensory brush cells of the trachea. A stable population in a dynamic epithelium. Am J Respir Cell Mol Biol 49:190–196

Sbarbati A, Osculati F (2005) A new fate for old cells: brush cells and related elements. J Anat 206:349–358

Sbarbati A, Tizzano M, Merigo F, Benati D, Nicolato E, Boschi F, Cecchini MP, Scambi I, Osculati F (2009) Acyl homoserine lactones induce early response in the airway. Anat Rec (Hoboken) 292:439–448

Schneider C, O'Leary CE, Locksley RM (2019) Regulation of immune responses by tuft cells. Nat Rev Immunol

Schneider C, O'Leary CE, von Moltke J, Liang HE, Ang QY, Turnbaugh PJ, Radhakrishnan S, Pellizzon M, Ma A, Locksley RM (2018) A metabolite-triggered tuft cell-ILC2 circuit drives small intestinal remodeling. Cell 174(271–284):e214

Schutz B, Jurastow I, Bader S, Ringer C, von Engelhardt J, Chubanov V, Gudermann T, Diener M, Kummer W, Krasteva-Christ G, Weihe E (2015) Chemical coding and chemosensory properties of cholinergic brush cells in the mouse gastrointestinal and biliary tract. Front Physiol 6:87

Spolarics Z (2007) The X-files of inflammation: cellular mosaicism of X-linked polymorphic genes and the female advantage in the host response to injury and infection. Shock 27:597–604

Ting HA, von Moltke J (2019) The immune function of tuft cells at gut mucosal surfaces and beyond. J Immunol 202:1321–1329

Tizzano M, Cristofoletti M, Sbarbati A, Finger TE (2011) Expression of taste receptors in solitary chemosensory cells of rodent airways. BMC Pulm Med 11:3

Tizzano M, Finger TE (2013) Chemosensors in the nose: guardians of the airways. Physiol (Bethesda) 28:51–60

Tizzano M, Gulbransen BD, Vandenbeuch A, Clapp TR, Herman JP, Sibhatu HM, Churchill ME, Silver WL, Kinnamon SC, Finger TE (2010) Nasal chemosensory cells use bitter taste signaling to detect irritants and bacterial signals. Proc Natl Acad Sci U S A 107:3210–3215

Voigt A, Hubner S, Doring L, Perlach N, Hermans-Borgmeyer I, Boehm U, Meyerhof W (2015) cre-mediated recombination in Tas2r131 cells-A unique way to explore bitter taste receptor function inside and outside of the taste system. Chem Senses 40:627–639

von Engelhardt J, Eliava M, Meyer AH, Rozov A, Monyer H (2007) Functional characterization of intrinsic cholinergic interneurons in the cortex. J Neurosci 27:5633–5642

von Moltke J, Ji M, Liang HE, Locksley RM (2016) Tuft-cell-derived IL-25 regulates an intestinal ILC2-epithelial response circuit. Nature 529:221–225

Wang JQ, Jeelall YS, Ferguson LL, Horikawa K (2014) Toll-like receptors and cancer: MYD88 mutation and inflammation. Front Immunol 5:367

Wiederhold S, Papadakis T, Chubanov V, Gudermann T, Krasteva-Christ G, Kummer W (2015) A novel cholinergic epithelial cell with chemosensory traits in the murine conjunctiva. Int Immunopharmacol

Yamamoto M, Yamaguchi R, Munakata K, Takashima K, Nishiyama M, Hioki K, Ohnishi Y, Nagasaki M, Imoto S, Miyano S, Ishige A, Watanabe K (2012) A microarray analysis of gnotobiotic mice indicating that microbial exposure during the neonatal period plays an essential role in immune system development. BMC Genomics 13:335

Yamamoto Y, Ozawa Y, Yokoyama T, Nakamuta N (2018) Immunohistochemical characterization of brush cells in the rat larynx. J Mol Histol 49:63–73

Yamashita J, Ohmoto M, Yamaguchi T, Matsumoto I, Hirota J (2017) Skn-1a/Pou2f3 functions as a master regulator to generate Trpm5-expressing chemosensory cells in mice. PLoS One 12:e0189340

Zheng R, Pan G, Thobe BM, Choudhry MA, Matsutani T, Samy TS, Kang SC, Bland KI, Chaudry IH (2006) MyD88 and Src are differentially regulated in Kupffer cells of males and proestrus females following hypoxia. Mol Med 12:65–73